Proceedings of the XVII ECSMGE-2019
Geotechnical Engineering foundation of the future
ISBN 978-9935-9436-1-3

doi: 10.32075/17ECSMGE-2019-0060

XVII European Conference
ECSMGE 2019
Reykjavik
on Soil Mechanics
and Geotechnical Engineering

Controlled desiccation behaviour of a clayey material based on digital image correlation DIC method

Comportement des sols argileux sous dessiccation contrôlée basé sur la technique de corrélation d'images numériques CIN

Lamine IGHIL AMEUR
Cerema Blois, Direction Territoriale Normandie-Centre, Blois, France

Mahdia HATTAB
Laboratoire d'études des microstructures et de mécanique des matériaux (LEM3 – UMR7239), Université de Lorraine, Metz, France

ABSTRACT: The aim of this research is to characterize the shrinkage phenomenon and analyze cracking mechanisms of a clayey soil subjected to the controlled desiccation in a laboratory experimental system. The approach consisted first to carry out a series of different controlled desiccation tests under three suction levels: high in 361MPa, middle in 110MPa and low in 38MPa on saturated remoulded clayey specimen with rectangular dimensions. Using the DIC method applied on captured and automatically saved images, total local strains were measured and devided in two parts: (a) the shrinkage strains which are only negatives and (b) the „mechanical" strains acting on the cracking and can be negatives or positives. When the „mechanical" strain increases and exceeds a defined critical value, cracks initiate and propagate through the surface of a soil sample.

RÉSUMÉ: L'objectif de cette étude est de contribuer à la compréhension du comportement global d'un sol argileux soumis à différents chemins de séchage contôlé. L'approche expérimentale consiste dans un premier temps à caractériser le phénomène de retrait puis analyser les mécanismes d'amorçage et de propagation des fissures de dessiccation. Des séries d'essais sous trois niveaux de succion imposée ont été réalisées : forte succion à 361MPa, moyenne succion à 110MPa et faible succion à 38MPa. Durant la phase d'essai, des images sont prises à interval défini et sauvegardées dans un PC pour permettre la mesures des déformations locales via la CIN. Une décomposition des déformations locales a été proposée définissant ainsi (a) une composante responsable du retrait toujours négative et (b) une composante „mécanique", positive ou négative, responsable de l'initiation et le développement des fissures.

Keywords: clay, shrinkage, cracks, critical strain, digital image correlation.

1 INTRODUCTION

The presence of cracks in a soil mass induces the creation of some zones of weak tension that drop down the mechanical resistance (Morris et al., 1992). Thus, this can have a significant impact on the hydraulic conductivity of clayey soils which increases with the development of cracks. Controlled desiccation is influenced by the atmospheric parameters that are relative humidity and temperature by a direct modification on drying variables such as water content, saturation degree, shrinkage limite and local suction of the soil.

Desiccation cracking of clayey soils usually occurred when the developed tensile stress due to suction exceeds the tensile strength of the soil (Kodikara et al., 1999). Tensile stresses develop only in the case where the soil is restricted against shrinkage. This restriction can be external due to the interface of a rough layer for example or internal due to some parts of soil during non-uniform drying for example.

Péron et al. (2009a) have investigated on the behaviour of cohesive soils under desiccation particularly on the shrinkage mechanisms and the initiation of cracks. Three kinds of desiccation tests were carried out: free desiccation tests, constrained desiccation tests (prevented shrinkage), and crack pattern tests. The results of two tests performed on two rectangular samples: (a) 300x300x4 mm^3 and (b) 300x300x12 mm^3 show a dense network of microcracks in (a) and a few large cracks in (b). Similar observations on squared samples were obtained in Corte and Higashi (1960). The formed angles by the cracks crossing were measured between 90° and 150° for all the tests.

Many researchers have given very important results on desiccation cracking, among of them: Lau (1987), Morris et al. (1992), Philip et al. (2002); Kodikara et al. (2002).

This research is mainly focused on the characterization of shrinkage phenomenon and understanding how controlled desiccation cracking initiate and propagate through a clayey materials. A series of controlled desiccation tests where then performed under three levels of imposed suction. The experimental approach consists to estimate shrinkage using DIC method and allows calculating a critical value of the mechanical local strain acting the cracking.

2 MATERIAL AND METHOD

2.1 Material properties and sample preparation

The tested clayey material in this study was Kaolinite K13 which is a synthetic clay close to be similar to the well known Kaolinite P300. Some of its physical properties are: liquid limit, $w_L = 40\%$; plastic limit, $w_P = 20\%$; density of the solid grains, $\gamma_s/\gamma_w = 2.65$; and shrinkage limit, $w_{SL} = 16\%$. As shown in Hattab et al. (2014), the elementary kaolinite particle is a set of stacked sheets.

In order to prepare the soil samples for controlled desiccation paths, Ighil Ameur (2016) performed tests by mixing dry powder of Kaolinite K13 with de-aired water at an initial water content, $w_0 = 1.2\ w_L$. The obtained slurry was then mixed and vibrated using a mixer apparatus during 15 minutes to remove air bubbles. Thus, the mixed slurry was let to settle for at least of 48 hours to ensure a homogeneous water content.

Soil sample was made by spreading mixed slurry on a rectangular teflon support with a dimensions of 190 mm in length, 130 mm in width and 4 mm in thickness as shown in Fig. 1.

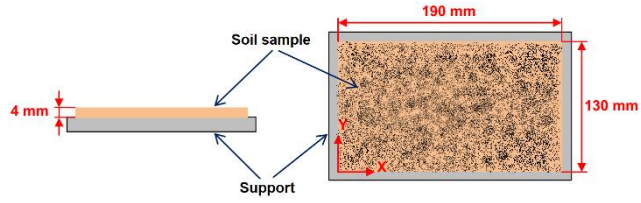

Figure 1. Soil sample preparation.

The upper surface of soil sample was subjected to be flecked with small and very dense spots of dark paint spraying. This was necessary for DIC calculations which need a different grey levels.

2.2 Test equipment

An experimental device (Fig. 2) was entirly developed to be able to combine two techniques for performing controlled desiccation tests: (i) a balance to follow water content evolution, salt solution to impose the hygrometric parameters (relative humidity and temperature) that were measured with a hygrometer; (ii) DIC method

which needs an HD camera to take images every fixed intervale, a computer to save the images and allows running calculations with Vic2D software.

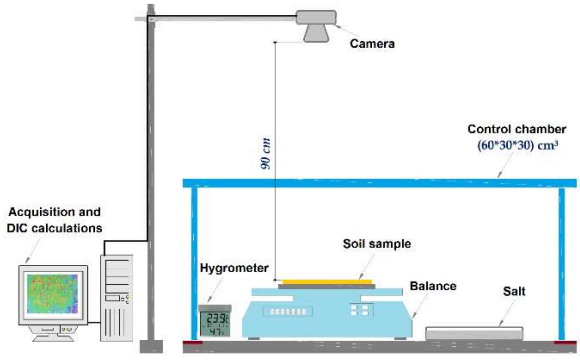

Figure 2. Experimental controlled desiccation test apparatus.

Fig. 2 shows that the soil sample is inside a control chamber of glass used to create a confined volume for applying salt solutions technique. Calibration tests were performed in Ighil Ameur (2016) to confirm that there is no glass-box effect on DIC calculations.

All the experimental device was placed in dark room where unique light was defined as shown in Fig. 3: LED 20W light projector, and large diffuse of white lighting using an umbrella.

Figure 3. Lighting conditions during test.

2.3 DIC method parameters

Before using Vic2D software, some parameters should be defined (Fig. 4): (i) scale calibration to convert pixels of saved images to milimiters of displacements, 1 pixel = 0.11 mm; (ii) subset = 17 and step = 5 of the selected area into the image, important parameters that allow to optimize DIC calculations in terms of the correlation quality and time needed to finish the run.

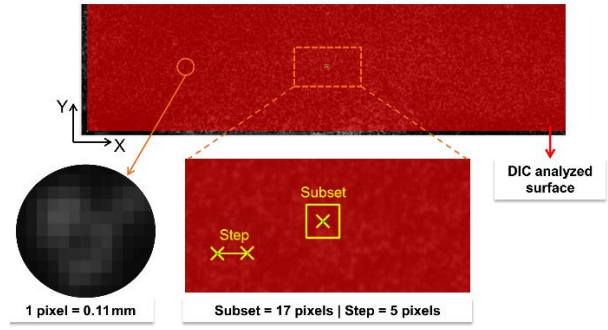

Figure 4. DIC parameters on Vic2D software.

The outputs of running Vic2D software are: (i) displacements, u (mm) along the X-axis, and v (mm) along the Y-axis; (ii) strains generated in post-processing, ε_{xx} (%) normal component of strain in the X-direction, ε_{yy} (%) normal component of strain in the Y-direction, and ε_{xy} (%) shear strain.

2.4 Salt solutions technique characteristics

Controlled desiccation tests were performed using salt solutions technique based on Kelvin's law given below:

$$u_a - u_w = \frac{RT}{gM_w} ln(RH\%) \qquad (1)$$

Where u_a and u_w (MPa) are air and water pressures, respectively. R (= 8.3143 J.mol^{-1}.K^{-1}) is the molar gas constant, T (°C) is temperature, g (= 9.81 m.s^{-2}) is the Earth's gravity, M_w (=18.016 g.mol^{-1}) is the molar mass, and RH (%)

is relative humidity. When T = 20°C, the constant $\frac{RT}{gM_w}$ equals 137.837 MPa.

Thus, equation (2) given in Fredlund and Rahardjo (1993) allows to determine the imposed global suction s_{glob} (MPa) as a function of RH and T:

$$s_{glob} = -\frac{\rho_w RT}{M_w} ln\left(\frac{RH\%}{100}\right) \qquad (2)$$

Where ρ_w (kg.m^{-3}) is the water density.

Three suction levels were fixed in this study corresponding to three salt solutions. The choice of salts was done according to the conditions cited in Delage et al. (1998): (i) the uncertainty of global suction Δs_{glob} given by the differential of Eq. 1 should be less than 15%; (ii) salts should have less sensibility than possible under temperature fluctuations.

Global suction and hygrometry of each salt solutions applied and faithful with conditions above are summarized in Table 1.

Table 1. Salt solutions applied for three suction levels

Salt	T (°C)	RH (%)	s_{glob} (MPa)
KOH	21.3	7±2	361±11
K2CO3	24.8	45±2	110±5.7
NaCl	24.4	75±2	38±9.8

Values of Table 1 are mean values because there are three tests realized for each suction levels. Test names are given following this nomenclature: CD (controlled desiccation)_Test number (1 to 3)_Mean value of s_{glob} (MPa). example: *CD2-s361* (test number 2 for high suction level).

3 RESULTS AND DISCUSSION

3.1 Hydric parameters evolution under controlled desiccation path

In order to analyze controlled desiccation behaviour of the tested soil, an example in Fig. 5 shows the evolution of hydric parameters as a function of time, t (hours) under middle suction level: (a) variations of water content, w and relative humidity, RH; (b) variations of global suction, s_{glob}.

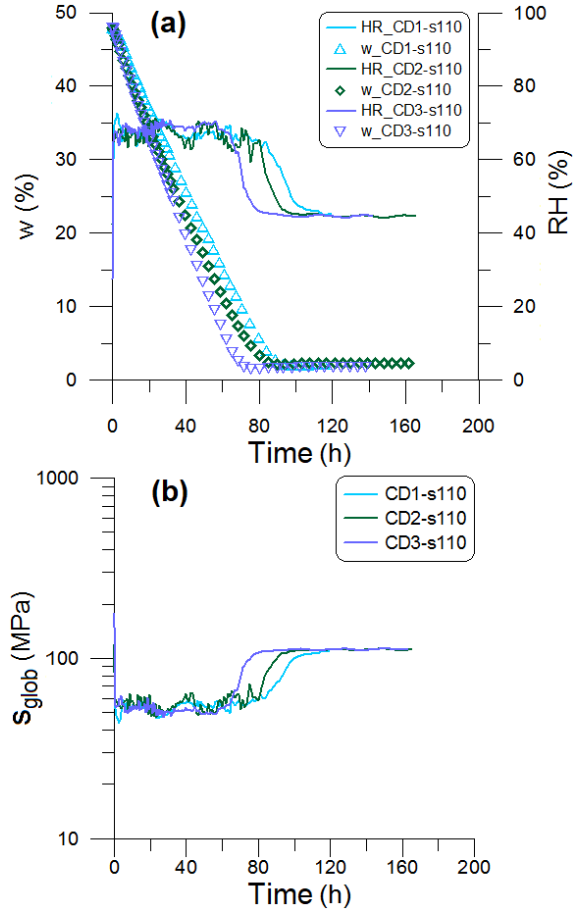

Figure 5. Hydric parameters variations under middle suction level.

Curves in Fig. 5 (a) show constant values of RH higher than the value that salt solution is supposed to impose (45%) during t = 80 h where w decreases. However, RH reached its theoretical value fixed by the salt when w is stabilized. Similar observations were noted under high and low suction levels. This can be explained by

water transfers between salt solution and the soil sample: (i) at the beginning of test, water transfers happened during vapor phase with saturated soil sample, where equilibrium didn't reached yet; (ii) as soon as soil sample desaturation is initiated, *RH* tends to its theoretical value and water transfers finalized at equilibrium state (Delage et Cui, 2000).

In the other hand, the results highlight a drying velocity $\frac{dw}{dt}$ (%/h) that changes with imposed suction level. Curves of Fig. 6 allow to identify 3 characteristic intervals of time: (i) from t_1 to t_2, mean value of drying velocity $\left(\frac{dw}{dt}\right)_m$ is determined; (ii) t_2 is the beginning of drying velocity decrease that tends to zero at t_3; (iii) for $t > t3$, $\frac{dw}{dt}$ equals zero then there is no drying which is equivalent to the stabilization of *w* curve in Fig. 5.

Therefore, these results show that there is an influence of global suction on drying velocity: more s_{glob} increases more $\frac{dw}{dt}$ is higher.

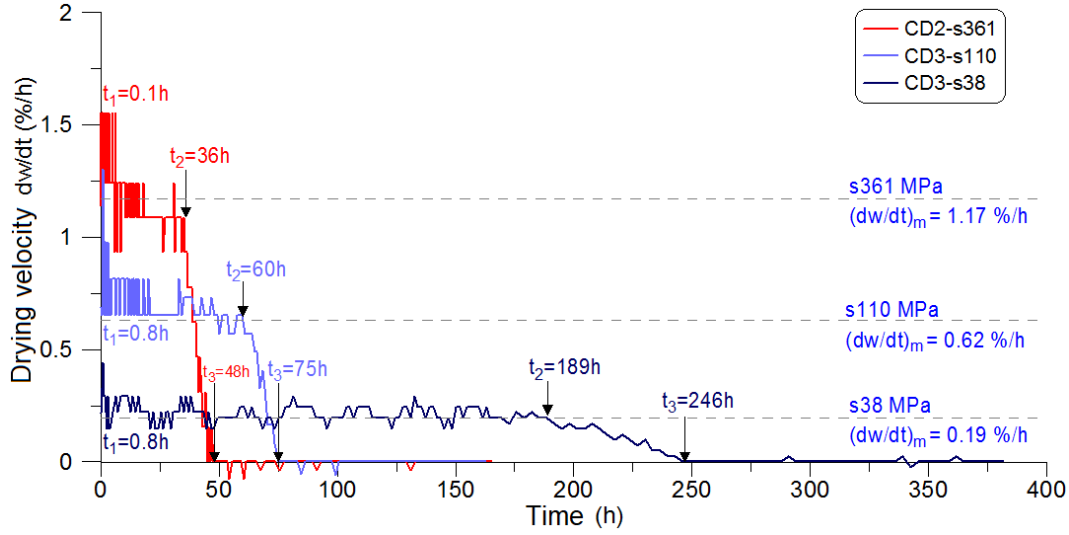

Figur 6. Shrinkage velocity under different suction levels during controlled desiccation path (m = mean values).

3.2 Shrinkage phenomenon: estimation

3.2.1 Analysis at the global scale

Shrinkage strain ε_{ss} is defined as a function of the volumetric strain ε_v following equation (3):

$$\varepsilon_{ss} = \frac{1}{2+\eta}\varepsilon_v \qquad (3)$$

Where $\eta = \frac{\varepsilon_z}{\varepsilon_h}$ is anisotropy ratio between vertical strain, ε_z and horizontal strain ε_h. Its experimental values are given in the literature: 2.5 in Péron et al. (2009a); > 2.0 in Auvray et al. (2014); and 2.0 in Wei et al. (2016).

Assuming that the strains are the same in both directions of horizontal plane ($\varepsilon_x = \varepsilon_y = \varepsilon_h$), volumetric strain become:

$$\varepsilon_v = \varepsilon_x + \varepsilon_y + \varepsilon_z = (2+\eta)\varepsilon_h \qquad (4)$$

Where ε_x and ε_y are global longitudinal and transversal strains, respectively. They are calculated with local strains ε_{xx} and ε_{yy} obtained from DIC method using Vic2D software. However, without local vertical strain ε_{zz} and no void ratio measures, ε_z is first estimated from SWCC curve in plane of void ratio as a function of water content $[e - w]$ given in Taibi (1994) and

Wei (2014). Then, the result was corrected according to ε_z evolution in Péron et al. (2009a). Thus, using these assumptions, ε_v was estimated by equation (4) and shrinkage was analyzed at the global scale in this study.

Shrinkage phenomenon is characterized by ε_v of the soil sample. Fig. 7 show the variations of ε_v as a function of time under the three suction levels where times at shrinkage limite t_{SL} are mentionned.

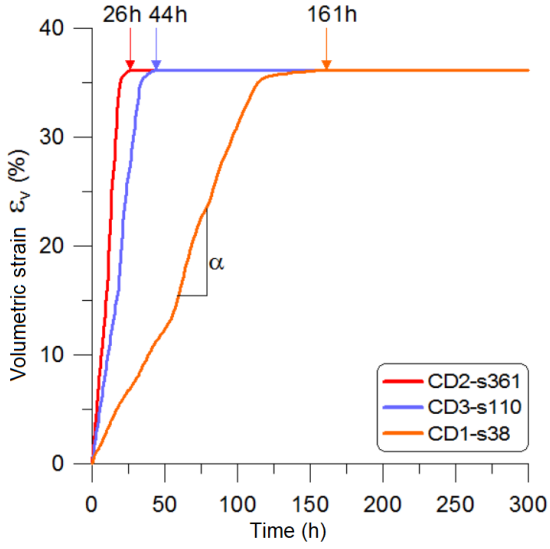

Figure 7. Global volumetric strain as a function of time under different suction levels.

Before time reached t_{SL}, the results show a linear increase of ε_v with a slope α which sensibly depends of suction level. α represente the shrinkage velocity defined by $\frac{d\varepsilon_v}{dt}$ during the phase where soil sample stays close the saturation ($t < t_{SL}$). Thus, Fig. 7 highlights that more suction level increases more shrinkage is fast and t_{SL} is very short.

3.2.2 Analysis at the local scale

Shrinkage phenomenon at the local scale is analyzed with DIC calculations and focused on an estimation of the local shrinkage strain ε_{ss}^{loc}. Displacement fields *u* and *v* obtained with Vic2D software under the three suction levels show that shrinkage is radial oriented to the center of soil sample as shown in Fig. 8.

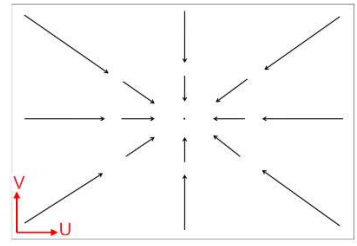

Figure 8. Local displacement fields orientation.

Based on the same assumptions as at the global scale, shrinkage is estimated at the local scale following equations (5) and (6) by estimating local vertical strain ε_{zz}:

$$\varepsilon_v^{loc} = \varepsilon_{xx} + \varepsilon_{yy} + \varepsilon_{zz} = (2+\eta)\varepsilon_h \qquad (5)$$

$$\varepsilon_{ss}^{loc} = \frac{1}{2+\eta}\varepsilon_v^{loc} \qquad (6)$$

Where ε_v^{loc} is the estimated local volumetric strain. Thus, a decomposition of local strains is proposed assuming: (i) first part of the negative strain is responsible of the shrinkage, ε^s; (ii) second part of the negative or positive strain is responsible of the initiation and propagation of desiccation cracking named "mechanical", ε^m:

$$\varepsilon_{xx} = \varepsilon_{xx}^s + \varepsilon_{xx}^m \qquad (7)$$

$$\varepsilon_{yy} = \varepsilon_{yy}^s + \varepsilon_{yy}^m \qquad (8)$$

$$\varepsilon_{zz} = \varepsilon_{zz}^s + \varepsilon_{zz}^m \qquad (9)$$

As example to highlight the importance of this decomposition for the local analysis, Fig. 9 shows logitudinal strain ε_{xx} maps under high suction level, CD2-s361; at $t = t_{SL} = 26$ h and $w = 17\%$. Several local zones noted from P1 to P10 are localized on the ε_{xx} maps. This analysis is focused on P3 zone, circled in red; and P8 zone circled in blue.

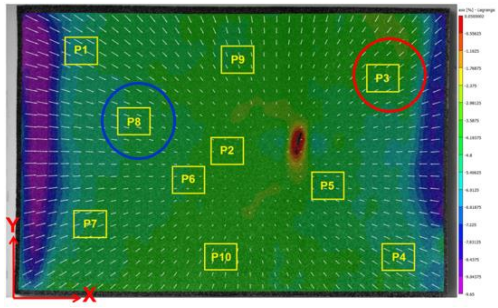

Figure 9. ε_{xx} maps – test CD2-s361 (t=26h; w=17%)

According to decomposition in equation (7), longitudinal strain components of zones P3 and P8 are ploted in Fig. 10 as a function of time. Negative values are compressions and positive values are extensions. Before $t = t_{SL}$, it is clearly shown a duality between shrinkage and mechanical components of ε_{xx}.

A peak in extension has identified in ε_{xx}^{m} curve at the beginning of test and changed to compression after. This could have given a crack.

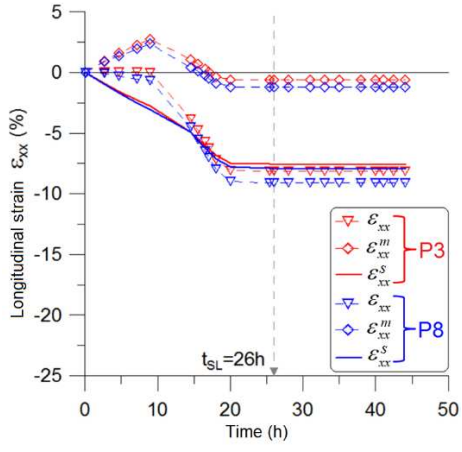

Figure 10. ε_{xx} components of zones P3 and P8.

3.3 *Discussion: controlled desiccation cracking*

Only mode I (opening mode) was observed in all cracks happened in this study under high suction level. Generally, cracks initiate from edges but some cracks can develop in the centre of soil sample due to an imperfection during its preparation (example can be observed in Fig. 9). are mentionned.

Two edge-cracking zones are localized on ε_{xx} and ε_{yy} maps shown in Fig. 11 and named III-CD2-s361 and II-CD2-s361, respectively. Time corresponds to the end of test t = 161 h and w = 2.65%.

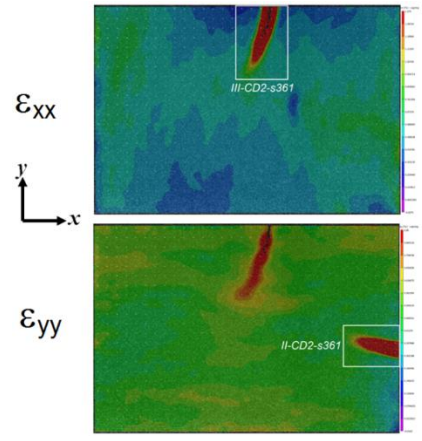

Figure 11. Identified cracks on ε_{xx} and ε_{yy} maps.

Fig. 12 shows the initiation and propagation of cracks above on ε_{xx} and ε_{yy} maps during drying. Crack III-CD2-s361 happened at t=42h and ε_{xx}^{m}= +0.724%. Crack II-CD2-s361 happened at t=40h and ε_{yy}^{m}= +0.612%.

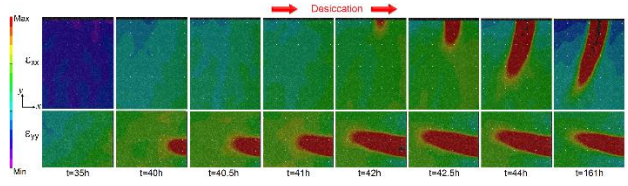

Figure 12. Cracks evolution during controlled drying.

4 CONCLUSIONS

In this research, an experimental device based on both salt solutions technique and DIC method was developed in the laboratory. This allowed to perform controlled desiccation paths under

different imposed suction levels. Study is focused on characterizing shrinkage phenomenon and understanding cracks‘ initiation and propagation.

Hydric parameters analysis showed that more imposed suction increases more drying velocity is higher.

Shrinkage phenomenon was estimated both at global and local scales. Its kinetic is influenced by imposed suction level similarly as for drying kinetic. In the other hand, its local analysis highlighted a decomposition of strain fields into shrinkage and „mechanical“ components.

Controlled desiccation cracking analysis shows that exceeding a defined critical value of „mechanical“ strain in extension, cracks initiate and propagate.

5 REFERENCES

Auvray R., Rosin-Paumier S., Abdallah A. & Masrouri F. (2014) "Quantification of soft soil cracking during suction cycles by image processing". Eur. J. Environ. Civ. Engng 18, No. 1, 11–32.

Corte A. and Higashi A. (1960) "Experimental research on desiccation cracks in soils". U.S. Army Snow Ice and Permafrost Research Establishment, Research Report No. 66, Corps of Engineers, Wilmette, Illinois, U.S.A.

Delage P., Howat M. D., Cui Y. J. (1998) "The relationship between suction and swelling properties in a heavily compacted unsaturated clay". Engineering Geology 50, 31–48.

Delage P. et Cui Y-J. (2000). "L'eau dans les sols non saturés". Techniques de l’Ingénieur. C301.

Fredlund D. G. and Rahardjo H. (1993) "Soil mechanics for unsaturated soils". John Willey, New York.

Hattab M., Hammad T., Fleureau J.M. (2014) Internal friction angle variation in a kaolin/montmorillonite clay mix and microstructural identification. Géotechnique 65(1):1–11.

Ighil Ameur L. (2016) Étude expérimentale du phénomène de l’endommagement et de la fissuration d’une matrice poreuse. Doctoral dissertation, Université de Lorraine, France.

Kodikara J. K., Barbour S. L., Fredlund D. G. (1999) "Changes in clay structure and behavior due to wetting and drying", proceedings of the 8th Australian-New Zealand Conference on Geomechanics, Hobart, p 179- 186.

Kodikara J. K., Barbour S. L., Fredlund D. G. (2002) "Structure development in surficial heavy clay soils: a synthesis of mechanisms", Australian Geomechanics, 37(3), 25–40.

Lau J. (1987) "Desiccation cracking of soils", Master thesis, Department of Civil Engineering, University of Saskatchewan, Canada.

Morris P. H., Graham J. and Williams D. J. (1992) "Cracking in drying soils". Canadian Geotechnical Journal 29: 263 – 277.

Péron H., Hueckel T., Laloui L. and Hu L.B. (2009a) "Fundamentals of desiccation cracking of fine-grained soils: experimental characterisation and mechanisms identification". Canadian Geotechnical Journal 46: 1177-1201.

Philip L. K., Shimell H., Hewitt P. J. and Ellard H. T. (2002) "A field-based test cell examining clay desiccation in landfill liners", Quarterly Journal of Engineering Geology and Hydrogeology, 35, 345–354.

Taïbi S. (1994) "Comportement mécanique et hydraulique des sols soumis à une pression interstitielle négative – Etude expérimentale et modélisation", Doctoral dissertation, Ecole Centrale Paris, France.

Wei X. (2014) "Etude micro-macro de la fissuration des argiles soumises à la dessiccation". Doctoral dissertation, Ecole Centrale Paris, France.

Wei X., Hattab M., Bompard P. and Fleureau J. M. (2016) "Highlighting some mechanisms of crack formation and propagation in clays on drying path". Geotechnique, 66(4), 287–300.